Molecular Therapy
Original Article

Reshaping the Immune Microenvironment by Oncolytic Herpes Simplex Virus in Murine Pancreatic Ductal Adenocarcinoma

Liming Zhang,[1,2] Wei Wang,[3] Ruikun Wang,[1,2] Nianchao Zhang,[2] Hang Shang,[1] Yang Bi,[1] Da Chen,[1] Cuizhu Zhang,[1,2] Long Li,[4,5] Jie Yin,[4,5] Hongkai Zhang,[1,3] and Youjia Cao[1,2]

[1]State Key Laboratory of Medicinal Chemical Biology and College of Life Sciences, Nankai University, Tianjin 300350, PR China; [2]Key Laboratory of Microbial Functional Genomics of Ministry of Education, College of Life Sciences, Nankai University, Tianjin 300071, PR China; [3]Shanghai Institute for Advanced Immunochemical Studies, ShanghaiTech University, Shanghai 201210, PR China; [4]Department of Immunology, Tianjin Medical University, Tianjin 300070, PR China; [5]Tianjin Medical University, Key Laboratory of Immune Microenvironment and Disease of the Ministry of Education, Tianjin 300070, PR China

Pancreatic ductal adenocarcinoma (PDAC) is the major type of pancreatic malignancy with very poor prognosis. Despite the promising results of immune checkpoint inhibitors (ICIs) in some solid tumors, immunotherapy is less effective for PDAC due to its immunosuppressive tumor microenvironment (TME). In this report, we established an immunocompetent syngeneic PDAC model and investigated the effect of oncolytic herpes simplex virus-1 (oHSV) on the composition of TME immune cells. The oHSV treatment significantly reduced tumor burden and prolonged the survival of tumor-bearing mice. Further, by single cell RNA sequencing (scRNA-seq) and multicolor fluorescence-activated cell sorting (FACS) analysis, we demonstrated that oHSV administration downregulated tumor-associated macrophages (TAMs), especially the anti-inflammatory macrophages, and increased the percentage of tumor-infiltrating lymphocytes, including activated cytotoxic CD8$^+$ T cells and T helper (Th)1 cells. Besides, the combination of oHSV and immune checkpoint modulators extended the lifespan of the tumor-bearing mice. Overall, our data suggested that oHSV reshapes the TME of PDAC by boosting the immune activity and leads to improved responsiveness of PDAC to immunotherapy.

INTRODUCTION

Pancreatic ductal adenocarcinoma (PDAC) is one of the most malignant cancers worldwide; once diagnosed, it is usually in the advanced stage, and the 5-year survival rate is about 9%.[1] Immune checkpoint inhibitors (ICIs), such as α-programmed cell death-1 (αPD-1)/PD-L1 and α-cytotoxic T-lymphocyte-associated protein 4 (αCTLA-4) antibodies (Abs), have achieved great progress in hematopoietic malignancies, as well as a number of solid tumors.[2–9] However, those treatments have poor efficacy toward PDAC due to the immune-excluded tumor microenvironment (TME) that composes immunosuppressive cells, i.e., the regulatory T cells (Tregs), myeloid-derived suppressor cells (MDSCs), tumor-associated macrophages (TAMs), and immunosuppressive cytokines.[10,11] Moreover, the TME of PDAC is filled with stromal fibroblasts and pancreatic stellate cells (PSCs) that form a physical barrier for the infiltrating lymphocytes, as well as ICI therapeutics.[12,13] The above factors lead to the irresponsiveness of PDAC to immunotherapy, and thus PDAC is considered an immunologically "cold" tumor. How to convert PDAC to be more susceptible to immunotherapy, namely the "hot" tumor, is the current challenge in the battle against pancreatic cancer.

Oncolytic virus is an alternative strategy to destroy the outgrowing tumor cells and thus increase the release of tumor-associated antigens (TAAs).[14] Meanwhile, infection of the oncolytic virus evokes the innate immune responses of cells in TME, which in turn activates the adaptive immune responses. In this regard, many engineered viruses have been developed for oncolytic therapies.[15–19] Herpes simplex virus 1 (HSV-1) is the most prevalent human virus and has been developed as one of the oncolytic viruses with minimum safety concern. For instance, HSV-1-derived talimogene laherparepvec (T-VEC; by Amgen, USA) has been approved by the US Food and Drug Administration (FDA) and European Medicines Agency (EMA) as the first oncolytic therapy for advanced melanoma, as well as many clinical trials worldwide for indications of glioma, head and neck cancer, and breast cancer.[20] For the characteristic TME of PDAC, it is crucial to understand the immunological effect of oncolytic HSV (oHSV) on PDAC.

Unlike human PDAC cells, the mouse PDAC cell line lacks the receptor for HSV-1. To investigate the HSV-based oncolytic therapy for PDAC, we established a new murine pancreatic cancer cell line, Pan02_herpes virus entry mediator (HVEM), which stably expressed

Received 1 May 2020; accepted 23 October 2020;
https://doi.org/10.1016/j.ymthe.2020.10.027.

Correspondence: Youjia Cao, State Key Laboratory of Medicinal Chemical Biology and College of Life Sciences, Nankai University, Tianjin 300350, PR China.
E-mail: caoyj@nankai.edu.cn
Correspondence: Hongkai Zhang, State Key Laboratory of Medicinal Chemical Biology and College of Life Sciences, Nankai University, Tianjin 300350, PR China.
E-mail: hongkai@nankai.edu.cn

the HVEM and verified that tumors developed successfully in the syngeneic mice by subcutaneous (s.c.) implantation of the cells. The intratumoral (i.t.) injection of oHSV significantly inhibited tumor growth and extended survival of tumor-bearing mice. By flow cytometry and single cell RNA sequencing (scRNA-seq) techniques, we profiled the composition of the immune cells in the tumor tissue and concluded that oHSV treatment enhanced tumor-infiltrating $CD8^+$ and $CD4^+$ effector T cells and increased the population of proinflammatory macrophages. In contrast, the existing immunosuppressive macrophages, neutrophils, and Tregs were reduced. The transcriptome profiling also revealed that PD-1, lymphocyte-activation gene 3 (LAG-3), and T cell immunoglobulin (Ig) domain and mucin domain 3 (TIM-3) were enriched in the $CD8^+$ T cell population, and tumor necrosis factor (TNF) receptor superfamily (TNFRSF), member 4 (OX40) and CTLA-4 were enriched in the $CD4^+$ T cell population. Accordingly, the combination of oHSV with anti-CTLA-4 and anti-OX40 antibodies significantly prolonged the survival of PDAC mice. Our studies shed light on the remodeling of the pancreatic TME by oHSV in an immunocompetent tumor model that may lead to the development of a therapeutic strategy by combining oHSV with immune modulators for PDAC.

RESULTS

Establishment of HSV-Infectible Murine PDAC Cells, Pan02_HVEM

First, we employed CRISPR-Cas9 system to genetically engineer the HSV-1 (F), resulting in a primary oHSV with deleted genes encoding ICP34.5 and ICP47 (Figure 1A). The construction of oHSV was verified by western blot and PCR (Figure S1).

Second, human PDAC cell lines were susceptible to HSV-1 and oHSV (Figures 1B–1D). However, both HSV-1 and oHSV were restricted in the C57BL/6 mice-derived PDAC cell line, Pan02 (Figure 1E), even though effective replication was seen in a colon cancer line of the C57BL/6 mice background, MC38 (Figure S2A). According to the Gene Expression Profiling Interactive Analysis 2 (GEPIA2) database, human pancreatic cancer cells highly express the HSV receptors, including HVEM, as we confirmed with human PDAC cell lines (data not shown). Thus, we established an infectible murine cell line stably expressing human HVEM, named Pan02_HVEM, as verified by fluorescence-activated cell sorting (FACS) analysis (Figure 1G). The oHSV efficiently infected and replicated in Pan02_HVEM cells, as confirmed with viral titration and viral protein expression (Figures 1F and 1H), although the viral replication efficiency was about 100-fold lower than in interferon (IFN)-incompetent Vero cells (Figure S2B).

oHSV Induced Cell Death and Cytopathology of Pan02_HVEM Cells *In Vitro*

The effect of oHSV infection on Pan02_HVEM cells was tested in parallel with HSV-1. Pan02_HVEM cells exhibited 49% and 25% cell death induced by wild-type HSV-1 and oHSV, respectively, whereas Pan02 cells remained intact (Figure 2A). In addition, interrupted cell proliferation appeared at 3 days postinfection (Figure 2B), and cytopathic effect (CPE) was observed in Pan02_HVEM cells but not in Pan02 cells (Figure 2C). Thus, the murine PDAC cell line, Pan02_HVEM, could be efficiently infected and lysed by oHSV *in vitro*.

oHSV Inhibited Tumor Growth in the Syngeneic Mouse PDAC Model

We s.c. inoculated Pan02_HVEM cells in C57BL/6 mice (defined as day 0) and treated them with purified oHSV on days 8, 11, and 14 (Figure 3A). On day 20, the mice were euthanized, and the tumors were resected. The oHSV treatment remarkably reduced tumor sizes and weights in comparison with the control (PBS) group (Figures 3B and 3C). We followed the tumor sizes in post-treated mice and observed tumor relapse along the withdrawal of oHSV treatment (Figures 3D and S3A). Nevertheless, oHSV treatment prolonged the survival of mice, as the median survival time was 31 days for the oHSV-treated group and 23 days for the control group, respectively (Figure 3E). We further examined the viral replication in tumor tissues and other loci and found that the replicative oHSV was detected in tumor tissues on day 15 (1 day after the last treatment), and no detectable viral particles were observed on days 17 and 20 in tumor tissues (Figure S3B). No virus was detected in liver and spleen tissues (data not shown). The restrained oHSV replication and deferred enlargement of the oHSV-treated tumor implicated that oHSV alone may not be sufficient to eliminate tumor cells in such an immune-competent model in which the prompt innate immune response to oHSV may lead to the relapse of tumor.

Furthermore, we characterized the anti-tumor effects of oHSV treatment using a bilateral tumor model. Briefly, Pan02_HVEM cells were inoculated on the right flanks of mice and the HSV nonpermissive tumor cells, Pan02, on the contralateral flanks of mice. When Pan02_HVEM tumors were treated with oHSV, the outgrowth of the tumors was inhibited (Figure 3F), consistent with the single-sided inoculation model in Figure 3B. Intriguingly, Pan02 tumors in the contralateral side were also restrained in oHSV-treated mice (Figure 3G). The abscopal effect of oHSV suggested an oHSV-induced systemic immune response contributing to the anti-tumor efficacy.

oHSV Treatment Enhanced the Immune-Stimulatory Cells in TME

Wild-type HSV-1 possesses mechanisms against host immune response; for instance, ICP34.5 blocks type I IFN secretion, and ICP47 interrupts TAP1-dependent antigen presentation.[21,22] Thus, the oHSV, with deletion of both *ICP34.5* and *ICP47*, is favorable to evoke the immune responses. We analyzed the immune cells of PADC by multicolor flow cytometry, of which, the gating strategy was shown in Figure S4. Indeed, oHSV treatment increased tumor-infiltrating leukocytes (TILs) (Figures 4A and 4B), particularly the $CD4^+$ T cells (Figure 4C). Although the proportion of $CD8^+$ T cells in the total TILs was not significantly (n.s.) changed in oHSV treated tumors (Figure 4D), the absolute numbers increased along with TILs. Tregs were dramatically reduced, and the ratio of $CD8^+$ T cells to Tregs increased in the oHSV treatment group compared with the

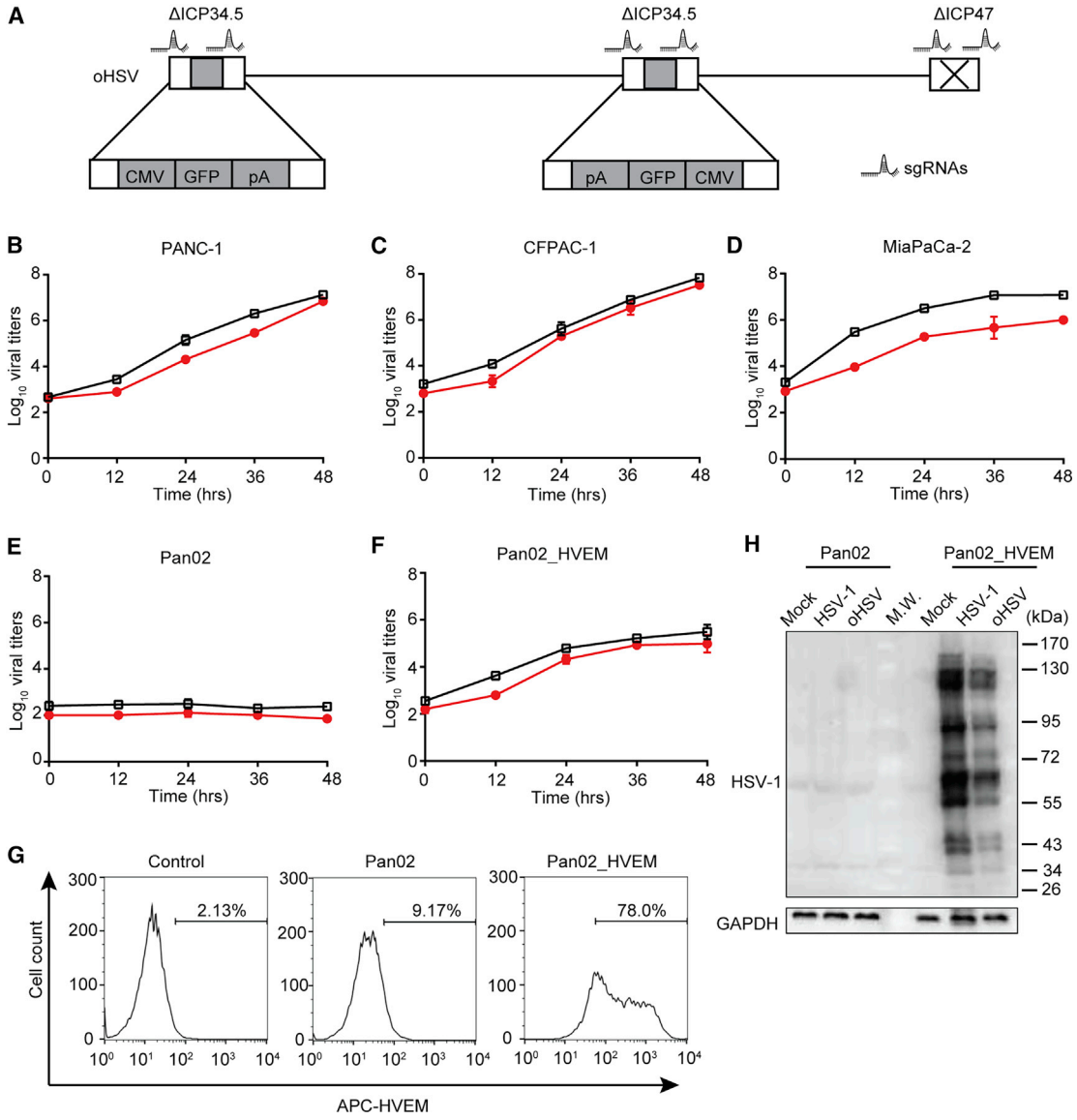

Figure 1. Susceptibility of PDAC Cell Lines to Oncolytic Herpes Simplex Virus (oHSV) Infection

(A) Schematic diagram of the engineered oHSV genome. By CRISPR-Cas9-based homologous recombination with two sets of sgRNAs, two copies of the *ICP34.5* gene were replaced by a GFP-expressing cassette, and *ICP47* was deleted. (B–F)Different cell lines PANC-1 (B), CFPAC-1 (C), MiaPaCa-2 (D), Pan02 (E), and Pan02_HVEM (F) were infected with wild-type HSV-1 (black squares) or oncolytic HSV (oHSV) (red circles) at MOI = 0.01, and the replication of viruses in those cell lines was determined by titration assays at the indicated time points. Viral titers were presented as Log pfu per mL and plotted on the vertical axis. (G) Pan02 and Pan02_HVEM cells were stained with APC-conjugated anti-HVEM antibody and then subjected to flow cytometry analysis. The histograms were shown with cell count as vertical axis and fluorescence intensity of APC as horizontal axis. The percentage of HVEM-positive cells was labeled inside. Control stands for Pan02 cells stained with APC-conjugated isotype IgG. (H) Pan02 and Pan02_HVEM cells were mock infected or infected with indicated viruses for 24 h. The expression of viral proteins was analyzed by western blot with antibodies against total HSV-1 proteins (top panel) or GAPDH as an internal loading control (bottom panel), respectively. (B–F) Data represented the mean values from three independent experiments with standard deviation. (G and H) Data were representative for three independent experiments.

control group (Figures 4E and 4F). In addition, the expression of IFN-γ in $CD4^+$ T cells and granzyme B (GZMB) in $CD8^+$ T cells was upregulated, respectively (Figures 4G and 4H), indicating the activation of both $CD4^+$ and $CD8^+$ T cells upon oHSV treatment. As noted, the expression of PD-1 in $CD8^+$ T cells was rather reduced upon oHSV treatment (Figure 4I), implying the limited efficacy of anti-PD-1 antibody therapy for PDAC.[23]

TAMs play important roles in building the immunological circumstance in tumors. Based on their effectiveness of inflammation,

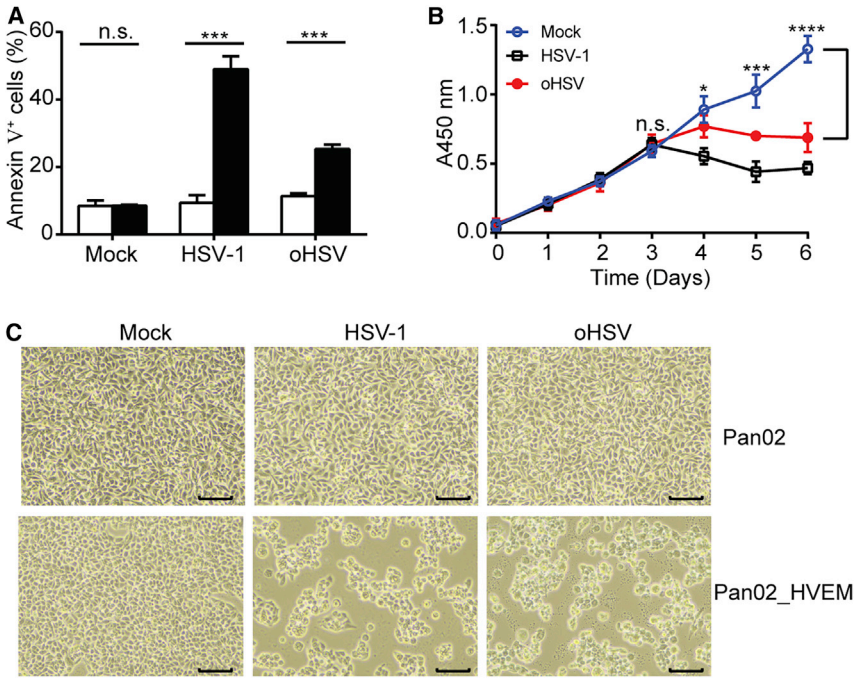

Figure 2. The Cytolytic Effects of oHSV

(A) Pan02 (open bar) and Pan02_HVEM (closed bar) cells were mock infected or infected with HSV-1 or oHSV at MOI = 1 for 24 h, stained with APC-conjugated Annexin V, and then subjected to flow cytometry analysis. The percentages of apoptotic cells (Annexin V^+) were plotted in columns. (B) Pan02_HVEM cells were mock infected (open circles) or infected with HSV-1 (open squares) or oHSV (closed circles) at MOI = 1, and cell proliferation was monitored by a CCK8 assay. The absorbance at wavelength of 450 nm was determined and plotted against time. Bracket, differences between mock-treated and oHSV-treated groups were statistically analyzed by two-tailed Student's t test. (C) Pan02 (top panels) and Pan02_HVEM (bottom panels) cells were mock infected or infected with indicated viruses at MOI = 1, and CPE on cells were observed at 24 hpi. Scale bar, 100 μm. The results were representative for three independent experiments. The data were expressed as the mean values with standard deviation (n = 3). Statistics analysis was performed using two-tailed Student's t test. n.s., not significant. *$p < 0.05$, **$p < 0.01$, ***$p < 0.001$, ****$p < 0.0001$.

macrophages are classified into two categories: proinflammatory (M1) and anti-inflammatory (M2) macrophages, respectively.[24,25] Intriguingly, upon oHSV treatment, the total macrophages marked as $CD11b^+F4/80^+/CD45^+$ seemed reduced by 13.48% (Figure 4J). The proinflammatory-like macrophages inducible nitric oxide synthase $(iNOS)^+$ remained unchanged, whereas the anti-inflammatory-like macrophages ($CD206^+$) decreased (Figures 4K and 4L). The oHSV treatment had no influence on the content of granulocytic (G)-MDSCs or monocytic (M)-MDSCs (Figures 4M and 4N). The major changes of T cells and macrophages were confirmed by immunohistochemistry of tumor samples (Figure S5). The above flow cytometry data suggested that oHSV treatment not only destroyed tumor cells directly but also shifted the TME balance toward more immunologically active.

To answer the question whether the immune balance of TME collapses eventually after oHSV therapy, we further monitored the composition of TILs as long as 32 days when all of the tumors reached 2,000 mm^3. As shown in Figure S6, on day 20, the oHSV-treated group exhibited higher level of $CD4^+$ T cells, whereas Tregs and anti-inflammatory-like macrophages were lower in the oHSV group than the control, respectively, as the data show in Figure 4. However, the contents of the oHSV treatment reduced Tregs and anti-inflammatory-like macrophages resumed on days 26 to 32, implicating a tumor relapse after the withdrawal of oHSV treatment.

Identification of PDAC-Infiltrated Immune Cells by scRNA-Seq Analysis

We next performed transcriptomic profiling by scRNA-seq with a 10× Genomics Platform to analyze immune cells in PDAC and identified 21 clusters (Figure 5A). By the characteristic markers, these clusters were identified as macrophages, T cells, natural killer (NK) cells, neutrophils, dendritic cells, and B cells (Figures 5A–5C). The oHSV treatment reduced proportions of macrophages in $CD45^+$ cells (Figure 5D). Meanwhile, the T/NK cell populations were significantly increased by more than 3-fold in the oHSV-treated group in comparison with the control group (Figure 5D).

oHSV Treatment Recomposed the i.t. Macrophages

Macrophages were the important players in TME and contributed more than one-half of total infiltrated immune cells in the murine PDAC model. scRNA-seq analysis displayed an overall profile based on the expression of *Nos2* as a marker of proinflammatory macrophages and *Mrc1* as a marker of anti-inflammatory macrophages. The expression of *Mrc1* decreased significantly following oHSV treatment (Figure 6A). The macrophage populations were further classified into 7 clusters (Mac_c1∼Mac_c7) (Figure 6B), and the distribution of each cluster was calculated in Figure 6C.

Cells in Mac_c1 and Mac_c7 had proinflammatory potential. Mac_c1 expressed a high level of major histocompatibility complex (MHC) class II transcripts (*H2-Aa*, *H2-Ab1*, *H2-Eb1*, *Cd74*), moderate level of *Nos2*, *Tnf*, *Cd83*, and *Cd86*, and low level of *Mrc1* and *Il10*. The oHSV infection upregulated the expression of the proinflammatory genes (Figure 6D). The proportion of this cluster of cells was raised from 17.75% to 23.82%. Mac_c7 was similar to Mac_c1, with a relatively low expression of the above genes, and the expression of *Nos2* also increased following oHSV treatment. In addition, these two clusters were marked with the upregulation of HSV-1 infection-associated pathways by Kyoto Encyclopedia of Genes and Genomes

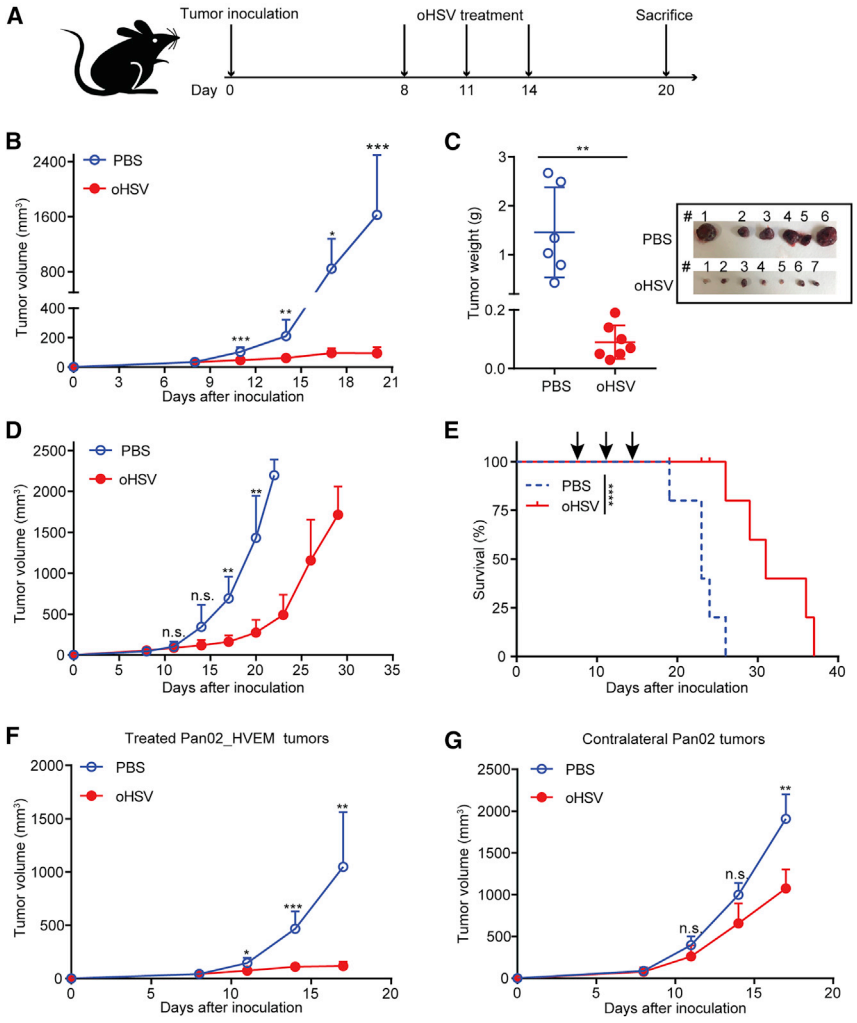

Figure 3. Oncolytic Effect of oHSV in the PDAC Syngeneic Mouse Model

(A) Schematic diagram of the oHSV treatment regimen. 5×10^5 Pan02_HVEM cells were implanted subcutaneously on day 0. oHSV or PBS was intratumorally injected on days 8, 11, and 14, respectively. Tumor volumes were measured every 3rd day following the first treatment. (B and C) After sacrificing the mice on day 20, the tumors were isolated (B), pictured (C, inset), and weighed (C). (D) The tumor growth curves of PBS- and oHSV-treated mice were shown until they exceeded 2,000 mm^3. On day 22, for the PBS control group, n = 3; on day 29, for the oHSV-treated group, n = 4. (E) The survival of tumor-bearing mice was plotted using Kaplan-Meier analysis (n = 5). 5×10^5 Pan02_HVEM cells were implanted subcutaneously into right flanks of mice, and 5×10^5 Pan02 cells were subcutaneously inoculated into the contralateral flanks of mice. PBS or oHSV was intratumoral injected into the Pan02_HVEM tumors on the right flanks, and the growth of the Pan02_HVEM tumor (F) and the distant Pan02 tumor (G) was shown. The tumor volumes were presented as mean values + standard deviation, and tumor weights were presented as mean values ± standard deviation and analyzed by Student's t test. Data for survival were analyzed by the log-rank test. *p < 0.05, **p < 0.01, ***p < 0.001.

(KEGG) analysis (Figure 6E). oHSV-induced elevation of *Nos2*, *Il1*, *Il6*, *Tnf*, *H2-Aa*, *H2-Ab1*, *H2-Eb1*, and *Cd74* was seen in Mac_c2. Besides, KEGG analysis showed that Mac_c2 cells possessed the signature of the hypoxia signaling pathway (Figure 6E), which may be related to macrophage polarization.[26]

Mac_c3∼Mac_c5 were regarded as immunosuppressive macrophages due to the high expression of *Mrc1* and *Il10*, which were decreased after oHSV treatment (Figure 6D). The percentage of these clusters decreased with oHSV treatment, specifically c3 from 16.65% to 4.56%, c4 from 6.43% to 1.34%, and c5 from 2.59% to 1.76% (Figure 6C). Moreover, KEGG analysis distinguished these clusters by the enrichment in the lysosome pathway and oxidative phosphorylation pathway (Figure 6E). In addition, Mac_c4 cells were rich in cell-cycle proteins and metabolic pathway (Figures 6D and 6E), indicating the active proliferating stage of macrophages.

The scRNA-seq results revealed that TAM activation states consist of a continuum of phenotypes. The classification of proinflammatory/anti-inflammatory phenotypes is simplistic to explain the heterogeneous and dynamic function of TAMs.[24,25] Nevertheless, the classification can be used to indicate the potential of macrophages being more proinflammatory or anti-inflammatory.

We further investigated the effect of $CD11b^+$ monocytes on PDAC with monocyte adoptive transfer assay. Briefly, the monocytes were isolated from PBS-treated mice (PBS-MCs) and oHSV-treated mice (oHSV-MCs), respectively, and then injected into tumor-carrying mice. The growth of tumors that received oHSV-MCs was hindered in comparison with that of PBS-MCs (Figure 6F). In addition, we assessed the effect of the above monocytes on $CD8^+$ T cell proliferation *in vitro* and found that PBS-MCs markedly suppressed the proliferation of $CD8^+$ T cells, whereas oHSV-MCs alleviated the suppressive effect of monocytes on T cells (Figure 6G).

Taken together, scRNA-seq analysis data revealed that oHSV treatment remodeled macrophage composition, especially decreasing the proportion of anti-inflammatory macrophages, and turned the immunosuppressive TME to be more proinflammatory. The adoptive cell transfer and T cell-proliferation assays indicated that the delay of tumor progression may be partly due to the change of monocytes induced by oHSV treatment.

oHSV Treatment Enhanced Tumor-Infiltrating Effector T Cells

The scRNA-seq analysis allowed further detailed profiling of the tumor-infiltrating lymphoid populations in PDAC. Twelve populations

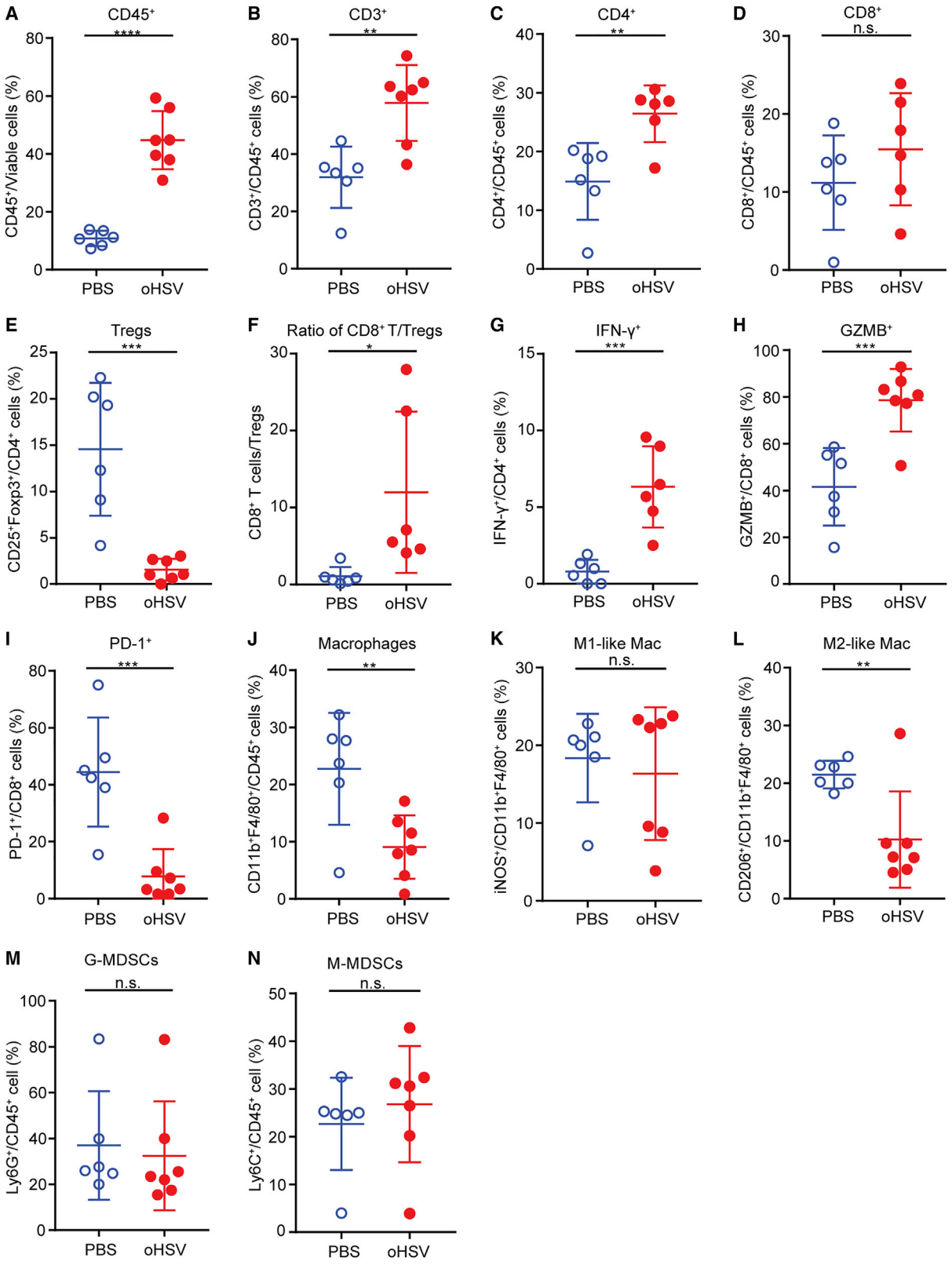

(legend on next page)

of lymphoid cells were defined as $CD8^+$ T cells, $CD4^+$ T cells, Tregs, NK cells, and γδ T cells (Figures 7A and 7C).

$CD8^+$ T cells were subdivided into 6 distinct clusters (CD8_c1∼CD8_c6) and classified into effector, memory, and exhausted T cells. CD8_c1 expressed a high level of *Tcf7*, *Ccr7*, *Sell*, *Lef1*, and *Fas*, indicating its central memory T (T_{CM}) phenotype,[27,28] and the percentage of which in total lymphoid cells decreased by 3-fold after oHSV treatment (Figures 7B and 7D). CD8_c2/c3 were identified as a mixture of effector/effector memory T cells based on the expression of markers, such as *Cd69*, *Klrg1*, but lack *Ccr7* and *Sell* (Figure 7D).[29] After oHSV treatment, the percentage of CD8_c3 was dramatically upregulated from 2.7% to 13.8% (Figure 7B). CD8_c2/c3 cells in the control group were characterized by no or low expression of *Ifng*, *Gzmb*, and *prf1*, whereas CD8_c3 of the oHSV-treated group were characterized by increased expression of *Ifng*, *Gzmb*, and *Prf1* and defined as activated cytotoxic T cells (Figures 7C and 7D). Cells in CD8_c4∼CD8_c6 represented active/exhausted T cells with reduced cytotoxic activity and elevated expression of immune checkpoint receptors. CD8_c6 was the least exhausted with relatively low expression of inhibitory receptors and high proliferation capability (Figure 7D). CD8_c5 cells were at the intermediate exhaustion stage with the intermediate expression of inhibitory receptors and reduced proliferation potential, regardless of the active oxidative phosphorylation metabolic state (Figures 7D and 7E). Upon oHSV treatment, the expression of immune checkpoint genes, such as *Pdcd1*, *Lag3*, *Havcr2*, and *Ctla4* in active/exhausted T cells, was reduced to a certain extent, suggesting that oHSV treatment may sustain the active phenotype of $CD8^+$ T cells.

Cluster 7 (CD4_c1) and cluster 8 (CD4_c2) were $CD4^+Foxp3^-$ conventional T cells (Tcon), and cluster 9 cells were $CD4^+Foxp3^+$ Tregs (Figures 7A and 7C). oHSV treatment led to a significant increase in the percentage of Tcon cells, particularly cells in CD4_c1 (Figure 7B). The gene-expression pattern of CD4_c1 represented primed T cells hallmarked by increased expression of *Cd28*, *Icos*, and *Cd40lg* (Figure 7D). CD4_c2 represented exhausted $CD4^+$ helper T (Th) cells, as indicated by the expression of *Pdcd1* and *Lag3*. Th cells consist of different subsets, such as Th1, Th2, and T follicular helper (Tfh) cell. The concomitant expression of Th1 lineage markers (interleukin [IL]-2 and IFN-γ) and Th2 lineage markers (IL-4, IL-13, and GATA3) in the control group suggests that Th1 and Th2 subsets coexisted.[30,31] Although upon oHSV treatment, the expression of Th2 lineage-specific marker genes dramatically dropped, transcripts of Th1 lineage markers (TNF) and Tfh lineage markers (BCL-6 and IL-21) were elevated in CD4_c2. Thus, oHSV treatment resulted in the polarization of the $CD4^+$ T cell toward Th1 and Tfh cells, whereas it negatively affected the expansion of pro-tumor Th2 lymphocytes. oHSV treatment caused a decrease of Tregs from 2.90% to 1.77%, and we found that Tregs expressed *Cd40lg* upon oHSV treatment (Figures 7B and 7D). The aberrant CD40L expression in Tregs could only be observed in severe inflammation.[32] Moreover, *Tbx21* expression in Tregs mediates a Th1-like response and contributes to inflammation rather than suppression phenotype.[33] All of these Th1-like responses manifested the functional reprogramming of Tregs by oHSV therapy.

We also defined NK cells (NK_c1, NK_c2) by the expression of *Ncr1* and *Klrb1c* (Figure 7C). Although the relative percentage of NK was reduced by oHSV treatment (Figure 7B), the NK cells were evidently stimulated by oHSV, as characterized by an elevated level of *Gzmb* and *Prf1* (Figure 7D). It is likely that oHSV promoted activation of NK cells, whereas it led to the reduction of cell numbers.

Cluster 12 was identified as γδ T cells for specifically expressing *Tcrg-C1* (Figure 7C). We also noted the expression of *Il17a* and *Rorc* induced by oHSV, representing the phenotype and function of innate-like IL-17-producing γδ T cells.[34]

The Combination Therapy of oHSV with Anti-CTLA-4 and Anti-OX40 Antibodies Prolonged the Survival of PDAC-Bearing Mice

The above scRNA-seq analysis revealed the gene-expression profile of T cells in the oHSV-treated PDAC model. We further extracted the expression patterns of the coreceptors of major T cells and analyzed the coexpression of *Pdcd1*, *Havcr2*, and/or *Lag3* in $CD8^+$ T cells (Figure 8A). Similarly, the expression of *Ctla4* and *Tnfrsf4* was presented in $CD4^+$ T cells (Figure 8B). These led to a hypothetical scenario that the oHSV treatment may proactively enhance the T cell responses and thus, the efficacy of the therapeutic antibodies of the coreceptors, such as PD-1, CTLA-4, etc. We then designed a superlative therapy by combining oHSV and therapeutic antibodies (Figure 8C).

As shown in Figure 8D, the survival of mice was monitored after treatments with oHSV plus isotype antibody as a control; tri-ICIs, including anti-PD-1, anti-TIM-3, and anti-LAG-3 antibodies; and the oHSV plus the three antibodies, respectively. Compared with the control (PBS) group, all of the treatments extended the median survival days from 18 to 23 (tri-ICIs only), 26 (oHSV alone), and

Figure 4. Effects of oHSV Treatment on Tumor-Infiltrating Immune Cells

Mice were subcutaneously implanted with 5×10^5 Pan02_HVEM cells and mock treated or treated with oHSV as described. Single cell suspension was prepared from tumor tissues on day 20 postinoculation. (A–N) Cells were then stained with fluorescence-conjugated antibodies and subjected to flow cytometry analysis for the contents of (A) $CD45^+$ cells; (B) $CD45^+CD3^+$ cells; (C) $CD45^+CD4^+$ T cells; (D) $CD45^+CD8^+$ T cells; (E) $CD4^+CD25^+Foxp3^+$Tregs; (F) the ratio of $CD8^+$ T cells to Tregs; (G) IFN-γ^+CD4^+ cells; (H) $GZMB^+CD8^+$ cells; (I) PD-1^+CD8^+ cells; (J) macrophages ($CD45^+CD11b^+F4/80^+$); (K) M1-like Mac ($CD11b^+F4/80^+iNOS^+$); (L) M2-like Mac ($CD11b^+F4/80^+CD206^+$); (M) M-MDSC ($CD45^+Ly6C^+$); and (N) G-MDSC ($CD45^+Ly6G^+$). The scatter graphs were plotted and presented as the percentage of an individual group of cells, as labeled on the vertical axis. Data were presented as mean values ± standard deviations, and statistics were analyzed using Student's t test. *$p < 0.05$, **$p < 0.01$, ***$p < 0.001$, ****$p < 0.0001$.

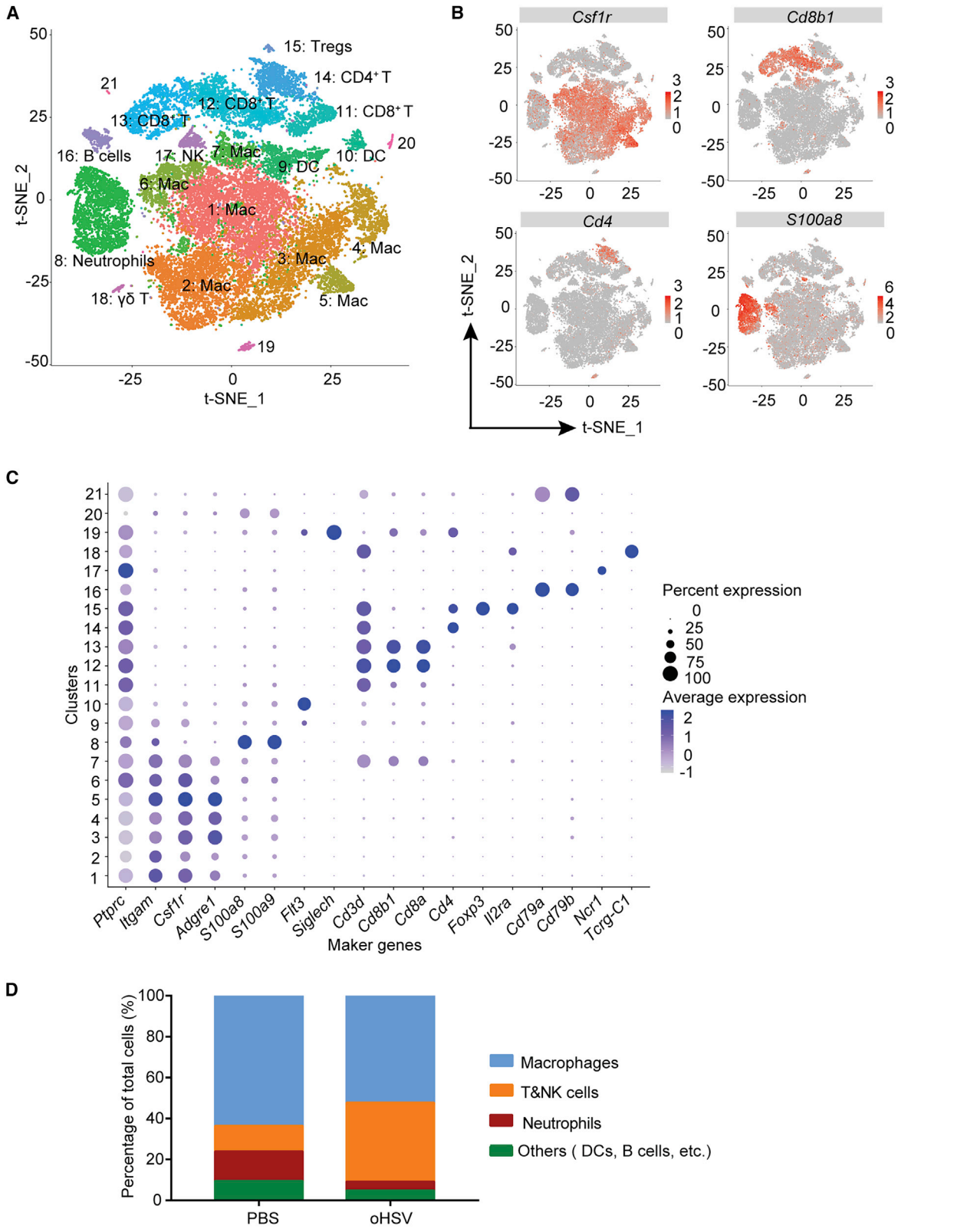

(legend on next page)

28.5 (combination) days, respectively. As a result, the tri-ICI-treated group had a modest effect on the immunocompetent PDAC mouse model (survived 5 more days), whereas the combination treatment of oHSV plus tri-ICIs showed little advantage over oHSV monotherapy. Notably, oHSV treatment exhibited better efficacy than tri-ICIs in this model.

On the other hand, the combination treatment of oHSV with anti-CTLA-4 antibody plus anti-OX40 agonist antibody significantly inhibited the growth of PDAC, with the median survival time of 36 days (Figure 8E) versus 30 days by oHSV alone. Interestingly, the treatment with antibodies only, anti-CTLA-4/anti-OX40 antibodies, had merely improvement on survival compared with the PBS group (25 days versus 22 days). Thus, oHSV, in combination with anti-CTLA-4 and anti-OX40 antibodies, achieved maximal survival of PDAC-bearing mice, and may be the optimal amelioration to the oHSV therapy.

Overall, the transcriptional profiling revealed that the oHSV infection activated cytotoxic $CD8^+$ T cells, induced the polarization of $CD4^+$ T cells toward Th1 effector cells, and activated NK cells in the PDAC tumor model. Intriguingly, the oHSV infection led to the reprogramming of the Tregs to execute a Th1-like helper response. All of these viral-induced variations contributed an immunological-active TME that potentially enhanced the tumor response to the immunotherapy. The investigation of oHSV-induced gene-expression patterns in TILs may guide the further designing of combination therapies to improve the efficacy toward PDAC.

DISCUSSION

Oncolytic viruses derived from HSV-1 have allured tremendous interests for cancer therapy since the characterization of ICP34.5 and ICP47.[35] With the FDA approval of T-VEC (Imlygic),[36] HSV-1 variants become a promising therapeutics to treat solid tumors. Here, we adopted the CRISPR-Cas9 technique to engineer the HSV-1, in which both copies of the *ICP34.5* coding region and *ICP47* gene were replaced or deleted (Figure 1A). The resulting oHSV was proven to induce cell death and CPE of mouse PDAC cell lines *in vitro* and inhibited the growth of the implanted tumor *in vivo* (Figures 2 and 3).

The xenografted models have been widely used to investigate the carcinogenesis and metastasis of human PDAC.[37–41] However, oncolytic virus treatment not only lysed the tumor cells per se but also induced immune responses in the interface of tumor cells and their living-by microenvironment. In this study, we established an oHSV-infectible murine PDAC cell line, Pan02_HVEM, and the syngeneic C57BL/6 mouse model. The implantation of the Pan02_HVEM cells showed no signs of immunogenicity or tissue rejection (data not shown). Another common model for PDAC is the KPC model, a genetically engineered mouse model, in which the mutant *Kras* and *Trp53* are expressed specifically in the pancreas.[42] The KPC model is ideal for the studies of PDAC tumorigenesis, whereas our model here emphasizes the immunological aspects in TME. Besides, for the KPC model, the *in situ* treatment of oHSV requires an injurious surgical procedure that likely evokes wound inflammation. To this measure, the s.c. tumor model that we developed is advantageous and practical to investigate the effect of oHSV on pancreatic TME.

Successful application of oHSV has been achieved in tumors with the manipulation of the immune microenvironment. For instance, IL-12-armed oHSV, G47Δ-mIL12, significantly decreases Tregs in glioblastoma.[43] Granulocyte-macrophage colony-stimulating factor (GM-CSF)-armed oHSV, $OncoVEX^{mGM\text{-}CSF}$, reduces the Treg population in melanoma and B lymphoma.[44,45] Apparently, these studies target Tregs, one of the major immunosuppressive players, to shift the immune balance of TME. Multiple lines of evidence revealed that the microenvironment of PDAC is immunosuppressive,[46,47] so that PDAC patients are insensitive to immunotherapies, such as anti-PD-1 or anti-CTLA-4 antibodies. With the primary version of the oHSV, we analyzed the components of TILs by scRNA-seq, without interference by additional cytokines. With respect to oHSV treatment, the overall tumor-infiltrating T/NK cells were increased (Figures 5D and 7B; CD8_c3 and CD4_c1). The anti-inflammatory-like macrophages and neutrophils were reduced, whereas the proinflammatory-like macrophages were elevated (Figures 5D and 6A). In agreement with the previous reports, the relative content of Tregs decreased (Figures 4E and 7B). Thus, the oHSV treatment alone, without armed cytokines, was able to convert the immunosuppressive TME toward more immune active.

Given the importance of TAMs in regulating tumor immunity, therapeutic strategies that target macrophages have the potential to augment the effect of the oncolytic virus. oHSV significantly reduced CSF1 receptor (CSF1R)-positive monocyte subsets Mac_c3∼Mac_c5 (Figures 6C and 6D) and partially overlapped with the effect of inhibition of CSF1R, which is intensively investigated in preclinical and clinical trials.[48] Besides TAM depletion, reprogramming TAMs toward an anti-tumor phenotype could be a more efficacious approach to enhance the efficacy of oHSV.

Figure 5. Tumor-Infiltrating Immune Cells Delineated by Single Cell RNA Sequencing (scRNA-Seq) Analysis

(A) The viable $CD45^+$ immune cells were isolated from tumor tissues of the PBS control mouse and oHSV-treated mouse using Microbeads, respectively. The scRNA-seq libraries of the leukocytes were prepared and sequenced. The scRNA-seq data were analyzed with Cell Ranger software. All immune cells from PBS and oHSV-treated tumors were clustered and represented as a t-distributed stochastic neighbor embedding (t-SNE) plot. Different clusters were color coded. (B) The expression of selected marker genes in total leukocytes was displayed in the t-SNE plot. Intensity of color was indicated for the level of expression. (C) Cell type-specific marker genes across all clusters were shown by bubble plot. Size of dots represented the fraction of cells expressing a particular marker, and intensity of color indicated the level of mean expression. (D) The components of tumor-infiltrating leukocytes were shown as percentage of total cells.

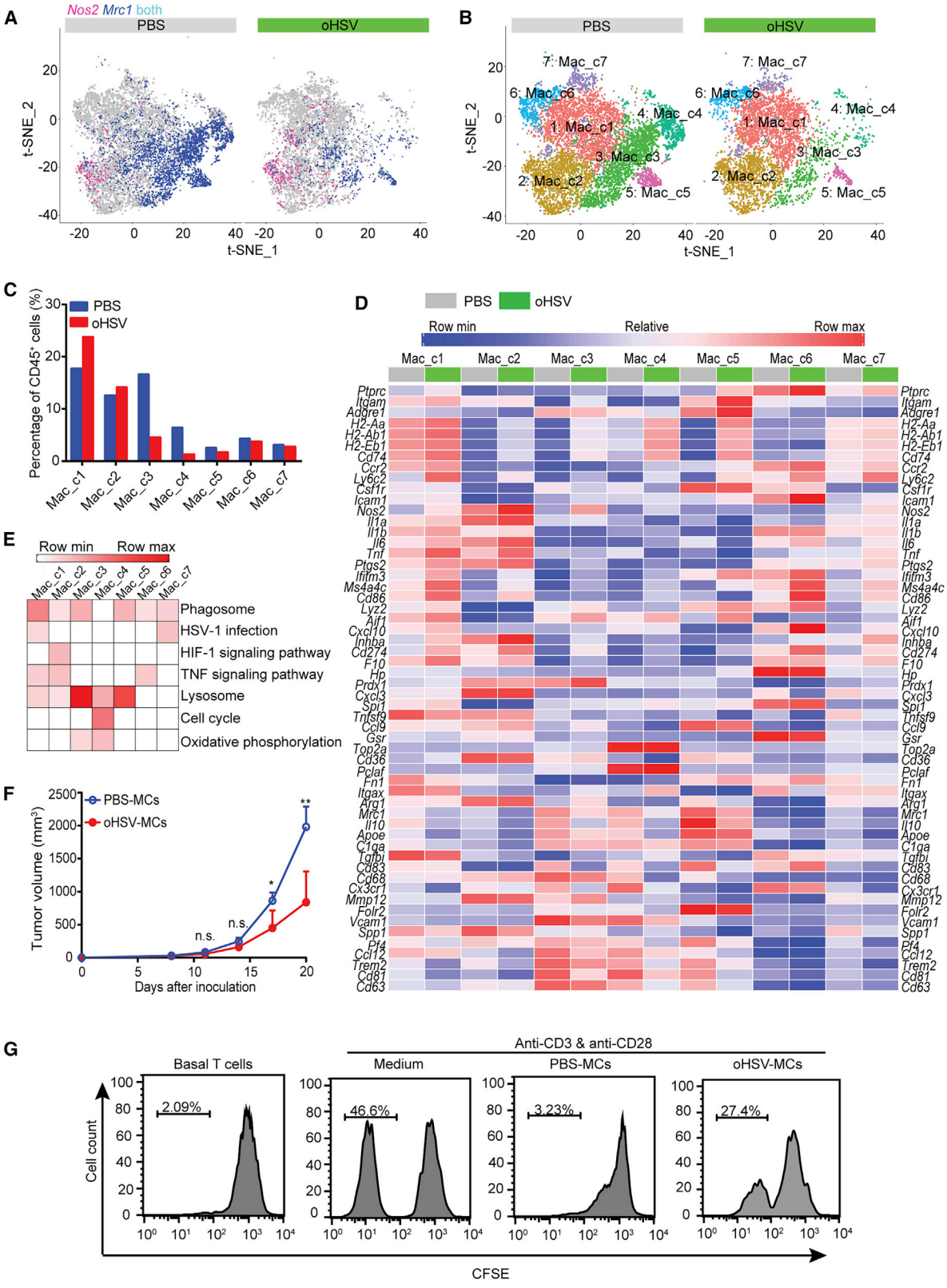

(legend on next page)

Despite the immune-stimulating effect of the oncolytic virus focused on in this study, we should also take the desmoplasia feature of the PDAC TME into account. The extracellular matrix (ECM) provides a physical barrier to inhibit penetration and dispersion of the oncolytic virus within tumor masses. A series of approaches have been attempted to partially degrade ECM proteins and improve the penetration of the oncolytic virus.[49] i.t. coinjection of collagenase or hyaluronidase with an oncolytic virus in human prostate and melanoma xenograft models increased i.t. viral spread and improved virus therapeutic efficacy.[50,51] A relaxin-expressing oncolytic adenovirus increased the i.t. distribution of virus by promoting the degradation of ECM.[52] A mouse model that recapitulates the hallmarks of PDAC in both the immune suppression and the desmoplasia would be of necessity to understand the effect of the oncolytic virus on different components of the TME.

Finally, the transcriptome profiling of this oHSV-treated mouse model provided not only the immune variation of PDAC TME but also a guidance for the further design of oHSV derivatives. It would also lead to combination strategies incorporated with immunotherapeutics to ameliorate the efficacy and combat tumor relapse. Based on the scRNA-seq analysis, we designed the combination therapy of oHSV with ICIs/agonists. Compared with oHSV monotherapy, in which the tumor relapsed after oHSV withdrawal, the combination of oHSV and anti-CTLA-4/anti-OX40 antibodies significantly prolonged the survival of PDAC-bearing mice (Figure 8E). However, little improvement was achieved with combination of oHSV and ICIs (Figure 8D). Perhaps the oHSV-induced expression of immune checkpoint genes, including PD-1, LAG-3, and TIM-3 on $CD8^+$ T cells, was insufficient to respond to ICIs in such a scenario. Further optimization would enhance the curative effects of oHSV and advise the designing of armed oHSV for PDAC.

In summary, we established an HSV-1-infectible murine pancreatic cancer cell line and developed a syngeneic PDAC model to explore the potential efficacy of oncolytic therapy. oHSV efficiently lysed tumor cells *in vitro*, reduced tumor burden, and prolonged survival *in vivo*. Importantly, oHSV increased the infiltration of effector T cells and downregulated immunosuppressive cells, thus turned the cold pancreatic TME into hot. The combination of oHSV and anti-CTLA-4/anti-OX40 antibodies significantly prolonged the post-treatment survival of the PDAC mice. This study may provide a rationale for the selection of immunotherapeutics in combination with oHSV for the treatment of PDAC.

MATERIALS AND METHODS

Cells and Viruses

PANC-1, CFPAC-1, MiaPaCa-2, HEK293T, MC38, and Vero cells were originally obtained from ATCC (VA, USA), and cultured in DMEM, supplemented with 10% (v/v) fetal bovine serum (FBS) and 1% penicillin/streptomycin. The murine PDAC cell line, Pan02, was purchased from Wuhan Union Hospital (Wuhan, PR China) and grew in RPMI-1640 medium containing 10% FBS and 1% penicillin/streptomycin. All cells were incubated at 37°C with 5% CO_2.

HSV-1 (F strain) was prepared in the lab as previously described.[53] The derived oncolytic virus oHSV with deletion of genes encoding ICP34.5 and ICP47 was obtained by CRISPR-Cas9-based homologous recombination. First, *ICP34.5* was replaced with the GFP-expressing cassette. The donor plasmid containing the homology arms of *ICP34.5* flanking the GFP-expressing cassette and the CRISPR plasmid containing the single guide (sg)RNAs of *ICP34.5* were cotransfected into HEK293T cells, followed by infection with the wild-type HSV-1. The produced viruses were harvested and the diluted viruses then infected Vero cells. The GFP^+ plaques were picked under fluorescence microscopy. The resulting *ICP34.5*-negative virus was confirmed by DNA sequencing and used for the next step of gene manipulation. Second, the *ICP47* gene of the *ICP34.5*-negative virus was replaced with the red fluorescent protein (RFP)-expressing cassette by a similar approach described above. Donor DNA containing the homology arms of *ICP47* flanking the RFP-expressing cassette and the CRISPR plasmid containing the sgRNAs of *ICP47* were cotransfected into HEK293T cells, followed by infection with the *ICP34.5*-negative HSV-1, and the produced viruses were harvested for infection of Vero cells. The RFP^+ plaques were picked under fluorescence microscopy. Finally, sgRNA-RFPs were applied to delete the *RFP* gene and made the *Us11* as an early expression gene. The resulting oncolytic virus was designated as oHSV, and the deletion of both *ICP34.5* and *ICP47* was verified by DNA sequencing, western blot, and RT-PCR.

Virus Propagation and Purification

Vero cells were infected with indicated viruses at a multiplicity of infection (MOI) = 0.01, and cells were collected at 48 h postinfection

Figure 6. Effect of oHSV Treatment on the Intratumoral Macrophages

(A) The expression of *Nos2* and *Mrc1* in tumor-associated macrophages from the PBS- and oHSV-treated group was shown by the t-SNE plot, respectively. Red, macrophages expressing *Nos2*; blue, macrophages expressing *Mrc1*. (B) Tumor-associated macrophages from PBS- and oHSV-treated tumors were clustered and displayed by the t-SNE plot, separately. Different macrophage clusters were color coded. (C) Cells in an individual cluster were plotted as percentage of $CD45^+$ cells. (D) Heatmap displayed the normalized expression of selected genes in an individual macrophage cluster from the PBS and oHSV treatment group, respectively. (E) Pathway enrichment in macrophage clusters. (F) $CD11b^+$ monocytes were isolated from tumor tissues of PBS (PBS-MCs)- and oHSV (oHSV-MCs)-treated mice on day 20, respectively, and the isolated cells were then intratumorally injected into Pan02_HVEM-bearing recipient mice. The tumor growth curve of the recipient mice was shown (n = 5). (G) $CD8^+$ T cells isolated from spleens of oHSV-treated mice were stained with CFSE and cocultured with medium or with the purified monocytes from PBS-treated mice (PBS-MCs) or oHSV-treated mice (oHSV-MCs) for 4 days in the presence of anti-CD3 and anti-CD28 antibodies, and the T cell proliferation was assessed by CFSE dilution assay. $^*p < 0.05$, $^{**}p < 0.01$.

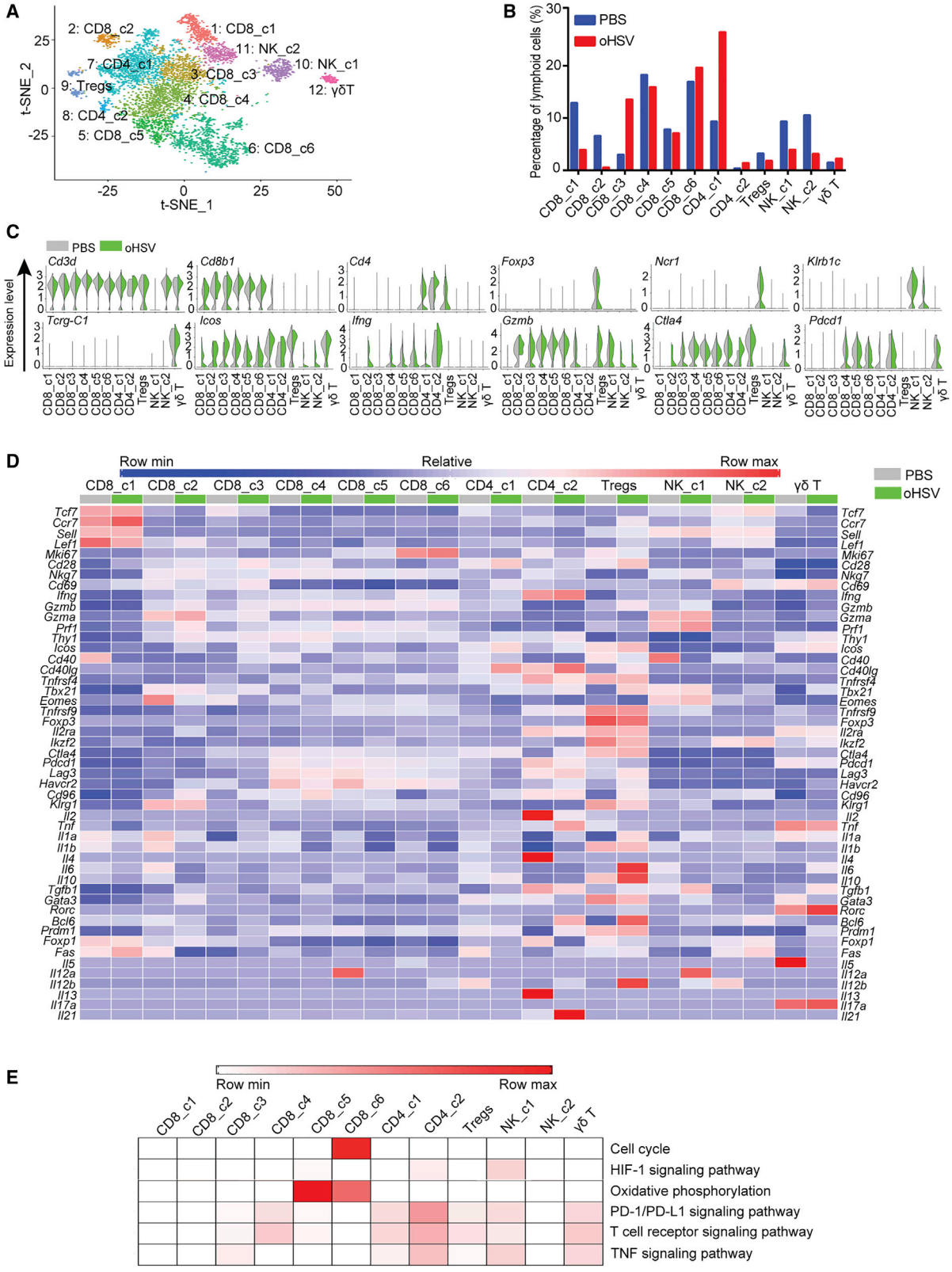

(legend on next page)

(hpi), then resuspended in sterile milk, frozen, and thawed three times. Samples were serial diluted, and the virus titers were titrated by oncolytic plaques on Vero cells.

The viruses were further purified for *in vivo* injection. Vero cells were infected with indicated viruses at MOI = 0.01. The cultured medium was collected at 72 hpi, and the supernatant went through the HiScreen Capto Core 700 (17-5481-15; GE Healthcare, NJ, USA) with an ÄKTA protein purification system to obtain the purified viruses. The purified viruses were then concentrated with an ultrafiltration tube (UFC910096; Millipore, MA, USA), and virus titers were measured by oncolytic plaques on Vero cells.

We used the Vero Cell HCP ELISA Kit (F500; Cygnus, MN, USA) to test the host residual protein of the purified viruses according to the manufacturer's protocol. Briefly, the samples, standards, and controls were pipetted into a 96-well plate and then an anti-Vero cell: horseradish peroxidase (HRP) was pipetted into each well and incubated on an orbital shaker for 2 h at room temperature. After washed four times, 3,3′,5,5′-tetramethylbenzidine (TMB) substrate was added to each well and incubated at room temperature for another 30 min, and the reaction was stopped by adding Stop Solution into each well. The absorbance at a wavelength of 450/650 nm was determined with a microplate reader (Synergy 4; BioTek).

Establishment of Pan02_HVEM Cells

Plasmid encoding human HVEM was obtained from Sino Biological (Beijing, PR China), and the coding region was amplified and inserted in the pCDH-CMV-MCS-EF1-Puro lentivector (provided by Dr. R. Xiang, Nankai University, Tianjin, PR China) at the EcoRI/BamHI cloning sites. All constructs were verified by DNA sequencing. The lentiviral particles were prepared with HEK293T cells, as described previously.[54] Basically, HEK293T cells were transfected with plasmids pCDH-CMV-HVEM-EF1-Puro together with pCMV-VSV-G, pMDLg/pRRE, and pRSV-REV. The viral particles were collected and incubated with Pan02 cells for 24 h and selected in the presence of puromycin (1.25 μg/mL) for 7 days, followed by flow cytometry sorting. The expression of HVEM was monitored by flow cytometry analysis with anti-HVEM antibody (MAB356; R&D Systems, MN, USA).

Western Blot Analysis

Western blot analysis for proteins was performed as described previously.[55] Briefly, the cultured cells were collected at 24 hpi and lysed with radioimmunoprecipitation assay (RIPA) buffer (25 mM Tris-HCl, pH 7.4, 150 mM NaCl, 5 mM EDTA, 1% Triton X-100, 10 mM PMSF, 1 mM NaF, 1 μg/mL leupeptin, 1 μg/mL pepstatin, 1 μg/mL aprotinin) on ice for at least 30 min, and the supernatants were then boiled in 6 × loading buffer (0.3 M Tris-HCl, pH 6.8, 12% SDS (m/v), 0.6% bromophenol blue, 36% glycerol, 6% β-mercaptoethanol [v/v]). Proteins were resolved by 12% SDS-PAGE; transferred to polyvinylidene fluoride (PVDF) membranes; and detected with indicated antibodies, anti-HSV-1 antibody (B0114; Dako Denmark A/S, CA, USA), and anti-glyceraldehyde 3-phosphate dehydrogenase (GAPDH) antibody (KM9002; Sungene, Tianjin, PR China).

CPE and Cell Death Analysis

To observe the CPE induced by viruses, cells were mock infected or infected with HSV-1 or oHSV at an MOI = 1, and images were taken under microscopy at 24 hpi. For cell death analysis, cells were mock infected or infected with indicated viruses at an MOI = 1, and cells were then collected, stained with allophycocyanin (APC)-conjugated Annexin V antibody (AO2001; Sungene, Tianjin, PR China), and subjected to flow cytometry analysis.

Cell Proliferation Assay

Cells were mock infected or infected with indicated viruses at an MOI = 1. At indicated time points, cells were incubated with Cell Counting Kit-8 (CCK8) (C6005; UE, Soochow, PR China) for 40 min at 37°C. The absorbance at wavelength of 450 nm was determined with a microplate reader (Synergy 4; BioTek).

Viral Titration Assay

Viral growth assay was performed as described.[53] Briefly, cells were infected with indicated viruses at an MOI = 0.01, and the medium-containing cells were collected at indicated time points, frozen, and thawed three times. Virus titers were measured as described above by serial dilutions and titrated by oncolytic plaques on Vero cells.

To measure viral growth *in vivo*, tumor tissues, livers, and spleens were dissected from tumor-bearing mice at the indicated time after therapies. The tissues were minced, homogenized, frozen, and thawed three times. The supernatants were collected by centrifugation and subjected to titration assay, as previously described.

Mice and PDAC Tumor Model

All animal experiments were performed in accordance with and approved by the Institute Research Ethics Committee of Nankai University. 5-week-old male C57BL/6 mice were obtained from Vital River Laboratories (Beijing, PR China). At 6 weeks of age, suspensions of 5×10^5 viable Pan02_HVEM cells in RPMI-1640 medium were s.c. implanted in mice, and the day of tumor inoculation was set as day 0. When tumor volumes reached approximately 50 mm^3, tumor-bearing mice were randomly divided into two groups, and i.t. treated

Figure 7. Effect of oHSV Treatment on Tumor-Infiltrating Lymphoid Cells

(A) Transcription information of tumor-infiltrating lymphoid cells was extracted from total immune cells data, then merged, and clustered by the t-SNE plot. Different lymphoid cell clusters were color coded as labeled. (B) Proportions of individual clusters were presented as percentage in total lymphoid cells of PBS- or oHSV-treated groups. (C) Violin plot showed specific gene expression in distinct lymphoid cell clusters of PBS- and oHSV-treated groups. (D) Heatmap displayed the normalized expression of selected genes in lymphoid cell clusters from PBS and oHSV treatment groups, respectively. (E) Heatmap of KEGG identified enrichment of pathways in clusters of lymphoid cells.

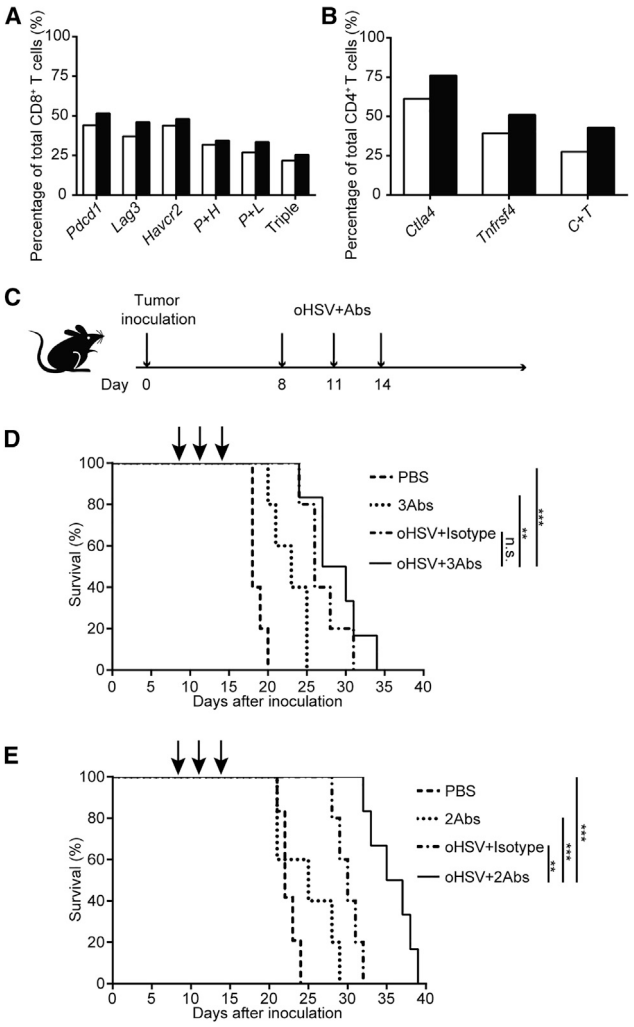

Figure 8. Combination Therapy of oHSV and Immune Checkpoint Inhibitors or Agonist

(A) The expression of immune checkpoint genes in $CD8^+$ T cells. *P + H*, cells coexpressed genes of *Pdcd1* and *Havcr2*; *P + L*, cells coexpressed genes of *Pdcd1* and *Lag3*; Triple, cells coexpressed the three genes of *Pdcd1*, *Havcr2*, and *Lag3*. Open bars, PBS control; closed bars, oHSV treated. (B) The expression of immune checkpoint genes in $CD4^+$ T cells. *C + T*, cells coexpressed genes of *Ctla4* and *Tnfrsf4*. Open bars, PBS control; closed bars, oHSV treated. (C) Schematic diagram of combination treatment regimen. Tumor-bearing mice were treated with oHSV or antibodies as indicated on days 8, 11, and 14. (D) The survival curve of tumor-bearing mice treated with PBS or 3 therapeutic antibodies (3Abs; anti-PD-1, anti-TIM-3, and anti-LAG-3 antibodies), or oHSV plus isotype antibody as control, or oHSV plus 3Abs as above. (E) The survival curve of tumor-bearing mice treated with PBS, or 2 antibodies (2Abs; anti-CTLA-4 plus anti-OX40 antibodies), or oHSV plus isotype antibody, or oHSV plus 2Abs as above. (D and E) PBS, Abs, and oHSV, n = 5; oHSV plus Abs, n = 6. Data for survival were analyzed by the log-rank test. $^*p < 0.05$, $^{**}p < 0.01$, $^{***}p < 0.001$.

with purified oHSV (1×10^7 plaque-forming units [PFU] per 100 μL per mouse) or PBS (100 μL per mouse) as control on days 8, 11, and 14 after tumor inoculation, respectively.

For the bilateral tumor model, 5×10^5 Pan02_HVEM cell suspension in RPMI-1640 medium was s.c. implanted on the right flanks of mice, and 5×10^5 Pan02 cells in RPMI-1640 medium were s.c. implanted on the contralateral flanks of mice. On day 8 post-tumor inoculation, tumors on right flanks were i.t. treated by PBS or oHSV every 3rd day for three times.

The length and width of tumors were measured every 3 days since the first treatment, and tumor volumes were calculated by formula V (mm^3) = length × $width^2/2$.

Therapeutic Administration and Survival

C57BL/6 mice were s.c. injected with 5×10^5 Pan02_HVEM cells, and tumor-bearing mice were randomly divided into groups on day 8. The mice were treated three times (days 8, 11, and 14 postinoculation) with indicated reagents, including PBS, oHSV, monoclonal antibodies against PD-1 (BE0146; Bio X Cell, NH, USA), TIM-3 (BE0115; Bio X Cell, NH, USA), LAG-3 (BE0174; Bio X Cell, NH, USA), CTLA-4 (BE0164; Bio X Cell, NH, USA), agonist antibody against OX40 (BE0031; Bio X Cell, NH, USA), and isotype control antibodies anti-IgG2a (BE0089; Bio X Cell, NH, USA) or anti-IgG1 (BE0088; Bio X Cell, NH, USA). The dose of oHSV was 1×10^7 PFUs per 100 μL per mouse, PBS was 100 μL per mouse, and each antibody was 100 μg per i.p. injection. When tumor volumes reached 2,000 mm^3, mice were sacrificed following the Animal Welfare Policy. The survival of tumor-bearing mice was monitored by Kaplan-Meier analysis.[56]

Dissociation of Single Cells from Tumor Tissues

Tumor tissues were harvested and minced from mice on indicated days and inoculated with dissociation solution (1 mg/mL collagenase I, 0.5 mg/mL DNase, 0.05 mg/mL Dispase II dissolved in PBS) for 1 h at 37°C with gentle shaking. After passing through 70 μm cell strainers and washed with RPMI-1640/2% FBS, the sample cells were resuspended in red blood cell lysis buffer (R1010; Solarbio, Beijing, PR China), followed by RPMI-1640 supplemented with 2% FBS.

Flow Cytometry Analysis

Mice were inoculated with viable Pan02_HVEM cells on day 0, and i.t. treated with PBS or oHSV on days 8, 11, and 14. Tumor-bearing mice were sacrificed on indicated days, and single cells from tumor tissues were first stained with viability dye (423106; BioLegend, CA, USA) at 4°C for 10 min; blocked with αCD16/32 antibody (101320; BioLegend, CA, USA) at 4°C for 10 min; and then stained with antibodies against mouse CD45 (103108; BioLegend, CA, USA), CD3ε (100328; BioLegend, CA, USA), CD4 (100428; BioLegend, CA, USA), CD8 (100752; BioLegend, CA, USA), CD25 (102036; BioLegend, CA, USA), PD-1 (135228; BioLegend, CA, USA), CD11b (101224; BioLegend, CA, USA), F4/80 (123114; BioLegend, CA, USA), CD206 (141732; BioLegend, CA, USA), Ly6C (128033; BioLegend, CA, USA), Ly6G (127639; BioLegend, CA, USA), intracellular staining with Foxp3 (320014; BioLegend, CA, USA), iNOS (12-5920-82; eBioscience, MA, USA), IFN-γ (505846; BioLegend, CA, USA), and GZMB (372208; BioLegend, CA, USA) following

the instruction of the True Nuclear Transcription Factor Buffer Set (424401; BioLegend, CA, USA) at 4°C for 40 min. Samples were then subjected to flow cytometry analysis, and data were analyzed using FlowJo software.

Immunohistochemistry Analysis

Mice were inoculated with Pan02_HVEM cells on day 0, and i.t. treated with PBS or oHSV on days 8, 11, and 14. Tumor tissues were isolated on day 20, fixed in 4% paraformaldehyde, and embedded in paraffin, and sections were immunostained with indicated primary antibodies against CD4 (25229; Cell Signaling Technology, MA, USA), CD8 (98941; Cell Signaling Technology, MA, USA), Foxp3 (12653; Cell Signaling Technology, MA, USA), F4/80 (70076; Cell Signaling Technology, MA, USA), iNOS (ab15323; Abcam, Cambridge, UK), and mannose receptor (ab64693; Abcam, Cambridge, UK) prior to the addition of biotinylated anti-rabbit Ig secondary antibodies.

Monocyte Adoptive Transfer

C57BL/6 mice were s.c. injected with 5×10^5 Pan02_HVEM cells on day 0, and i.t. treated with PBS or oHSV on days 8, 11, and 14. The $CD11b^+$ monocytes were isolated from tumor tissues of PBS- and oHSV-treated mice on day 20 using CD11b Microbeads (130-126-725; Miltenyi Biotec, Bergisch Gladbach, Germany), according to the manufacturer's protocol, respectively. 5×10^5 purified $CD11b^+$ monocytes were then adoptively transferred into Pan02_HVEM-bearing recipient mice (day 8 post-tumor cell inoculation) by i.t. injections. The tumor volumes were measured every 3 days.

T Cell Proliferation Assay

C57BL/6 mice were s.c. injected with 5×10^5 Pan02_HVEM cells on day 0, and i.t. treated with PBS or oHSV on days 8, 11, and 14. $CD8^+$ T cells were enriched from spleens of oHSV-treated mice on day 20 by the $CD8a^+$ T Cell Isolation Kit (130-104-075; Miltenyi Biotec, Bergisch Gladbach, Germany), according to the manufacturer's protocol. The isolated cells were stained with 6 μM carboxyfluorescein diacetate succinimidyl ester (CFSE; 565082; BD, NJ, USA) for 10 min, and the labeled $CD8^+$ T cells were cocultured with/without the purified monocytes (isolated from tumor tissues on day 20) at a ratio of 1:1. Cells were stimulated with well-coated anti-CD3 (102111; BioLegend, CA, USA) and anti-CD28 (100208; BioLegend, CA, USA) antibodies for 4 days, and the proliferation of $CD8^+$ T cells was assessed by CFSE dilution assay with flow cytometry analysis.

Preparation for scRNA-Seq Library

Tumor-bearing mice treated by PBS and oHSV were killed (n = 1) on day 20 post-tumor inoculation, tumors were digested into single cells, and the viable $CD45^+$ immune cells were sorted from single cell suspensions by the Dead Cell Removal Kit (130-090-101; Miltenyi Biotec, Bergisch Gladbach, Germany) and CD45 (TIL) Microbeads (130-110-618; Miltenyi Biotec, Bergisch Gladbach, Germany) ordinally, according to the manufacturer's protocol. Cells were adopted only when their viabilities were more than 85%. The following experiments were manipulated by Bio Miao Biological Technology (Beijing, PR China), according to the manufacturer's protocol (10× Genomics). Briefly, two independent single cell suspensions from PBS- and oHSV-treated tumors were loaded onto the 10× Genomics Chromium Platform to generate Gel Beads-in-Emulsion (GEM) at the concentration about 1,000 cells/μL for totally about 20,000 cells per sample. After the GEM generation, the samples were incubated at 53°C for 45 min and 85°C for 5 min in Thermal Cycle (C1000; Bio-Rad) to barcode the cDNA. GEMs were then broken, and the cDNA was purified by Dynabeads MyOne Silane Beads and amplified (98°C for 3 min, followed by 16 cycles: 98°C for 12 s, 63°C for 20 s, 72°C for 60 s, and followed by 72°C for 1 min). An Agilent Bioanalyzer 2100 was used to assess the quality of cDNA. cDNA was fragmented, end-repaired, a-tailed, then subjected to a double-sided size selection with SPRIselect beads and ligated to adaptors. cDNA was then amplified with the following parameters: 98°C for 45 s, followed by 14 cycles: 98°C for 20 s, 54°C for 30 s, 72°C for 20 s, and followed by 72°C for 1 min. The constructed libraries were subjected to double-sided size selection again, and the quality of the libraries was also assessed. Then libraries were sequenced using an Illumina NovaSeq 6000 sequencer with the paired-end 2 × 125 base pair (bp) sequencing standard.

Data Processing and Analysis

The Cell Ranger software (version [v.]3.1.0) was downloaded from the 10× Genomics website https://support.10xgenomics.com/single-cell-dna/software/release-notes/1-1#header https://support.10xgenomics.com/single-cell-gene-expression/software/downloads/latest., and mouse reference dataset (mm10-3.0.0) was also downloaded from the 10× Genomics website https://cf.10xgenomics.com/supp/cell-exp/refdata-cellranger-mm10-3.0.0.tar.gz. For each individual sample's FASTQs, the Cell Ranger count module with default parameters was used to align, filter, count barcodes, and count unique molecular identifiers (UMIs). Finally, we generated a gene-barcode matrix containing the barcoded cells and gene-expression counts for each sample.

Identification of Cell Types and Cluster Marker Genes in Seurat

Gene-barcode matrices were imported into the Seurat pipeline for quality control and downstream analysis.[57] Low-quality cells (<500 genes/cells, >8,000 genes/cells, >10% mitochondrial) and suspectable populations of doublet were excluded. The data were then normalized, and most variable genes were detected by the FindVariableFeatures function. Then samples' Seurat objects were combined together by canonical correlation analysis (CCA). Principal-component analysis (PCA) was performed on about 4,000 of the most variable genes with PCA function, and the first 50 PCA components were used for graph-based clustering (at a resolution of 0.5) to identify distinct types of cells. These cell types were projected onto the t-distributed stochastic neighbor embedding (t-SNE) analysis run using previously computed 50 PCA components. To determine lymphoid cells, cells expressing *Cd3d* and *Ncr1* were extracted from total samples, and cell types were projected onto the t-SNE analysis run.

We used the FindAllMarkers function in the Seurat pipeline to characterize the cluster-specific marker genes, and to identify differentially expressed genes (DEGs) between two clusters, we used the FindMarkers function. The average expression of the markers within each cluster was calculated, and the heatmaps of marker gene average expression were generated by R package ComplexHeatmap.[58]

Pathway Enrichment Analysis

For each cluster, only the genes expressed in more than 10% of the cells with at least 0.25-fold difference and at most 0.05 adjusted p value were considered as DEGs in each cluster. We used R package clusterProfiler to perform pathway enrichment analysis for each cluster's DEGs.[59]

Statistical Analysis

The quantitative data were presented as mean value ± standard deviation (SD) of at least three independent experiments. Data were analyzed using two-tailed Student's t test.[60] Animal survival was presented using Kaplan-Meier survival curves, and data for survival were analyzed by the log-rank test.[56] A p value that was less than 0.05 (*) was considered to be statistically significant (*$p < 0.05$, **$p < 0.01$, ***$p < 0.001$, and ****$p < 0.0001$).

SUPPLEMENTAL INFORMATION

Supplemental Information can be found online at https://doi.org/10.1016/j.ymthe.2020.10.027.

AUTHOR CONTRIBUTIONS

Y.C. and H.Z. conceived the study. L.Z., H.Z., and Y.C. designed all experiments, analyzed all of the data, and wrote the manuscript with the input of all authors. L.Z. and R.W. performed the experiments. N.Z., H.S., Y.B., D.C., and C.Z. assisted with the viral preparation, infection, and titration. L.Z., J.Y., and L.L. performed FACS data analyses. L.Z., W.W., and H.Z. interpreted the scRNA-seq data.

CONFLICTS OF INTEREST

The authors declare no competing interests.

ACKNOWLEDGMENTS

The authors would like to thank Drs. Bin He (UIC, USA) for providing relevant information about the HSV-1 genome and critical suggestions; Xianwen Ren (Peking University, China) and Lichun Jiang (ShanghaiTech University, China) for providing relevant information about single cell RNA sequencing data analysis; and Jun Chen (Sun Yat-Sen University, China) for providing suggestions on assays for monocytes. This work was supported by the National Natural Science Foundation of China (grant numbers 81661148051 and 81672010 to Y.C. and 81872787 to H.Z.); Programme of Introducing Talents of Discipline to Universities (grant number B08011); Fundamental Research Funds for the Central Universities, Nankai University (grant number ZB19100123); Open Fund of the State Key Laboratory of Medicinal Chemical Biology for Tianjin Stomatological Hospital; National Natural Science Foundation of China (grant 31600705 to J.Y.); and Tianjin Natural Science Foundation (grant 17JCQNJC09000 to J.Y.).

REFERENCES

1. Siegel, R.L., Miller, K.D., and Jemal, A. (2020). Cancer statistics, 2020. CA Cancer J. Clin. *70*, 7–30.
2. Chen, R., Zinzani, P.L., Fanale, M.A., Armand, P., Johnson, N.A., Brice, P., Radford, J., Ribrag, V., Molin, D., Vassilakopoulos, T.P., et al.; KEYNOTE-087 (2017). Phase II study of the efficacy and safety of pembrolizumab for relapsed/refractory classic hodgkin lymphoma. J. Clin. Oncol. *35*, 2125–2132.
3. McClanahan, F., Riches, J.C., Miller, S., Day, W.P., Kotsiou, E., Neuberg, D., Croce, C.M., Capasso, M., and Gribben, J.G. (2015). Mechanisms of PD-L1/PD-1-mediated CD8 T-cell dysfunction in the context of aging-related immune defects in the Eμ-TCL1 CLL mouse model. Blood *126*, 212–221.
4. Ribas, A., Dummer, R., Puzanov, I., VanderWalde, A., Andtbacka, R.H.I., Michielin, O., Olszanski, A.J., Malvehy, J., Cebon, J., Fernandez, E., et al. (2017). Oncolytic virotherapy promotes intratumoral T cell infiltration and improves anti-PD-1 immunotherapy. Cell *170*, 1109–1119.e10.
5. Sun, L., Funchain, P., Song, J.M., Rayman, P., Tannenbaum, C., Ko, J., Mcnamara, M., Marcela Diaz-Montero, C., and Gastman, B. (2018). Talimogene Laherparepvec combined with anti-PD-1 based immunotherapy for unresectable stage III-IV melanoma: a case series. J. Immunother. Cancer *6*, 36.
6. Ahmed, K.A., Kim, S., Arrington, J., Naghavi, A.O., Dilling, T.J., Creelan, B.C., Antonia, S.J., Caudell, J.J., Harrison, L.B., Sahebjam, S., et al. (2017). Outcomes targeting the PD-1/PD-L1 axis in conjunction with stereotactic radiation for patients with non-small cell lung cancer brain metastases. J. Neurooncol. *133*, 331–338.
7. Tahara, M., Muro, K., Hasegawa, Y., Chung, H.C., Lin, C.C., Keam, B., Takahashi, K., Cheng, J.D., and Bang, Y.J. (2018). Pembrolizumab in Asia-Pacific patients with advanced head and neck squamous cell carcinoma: Analyses from KEYNOTE-012. Cancer Sci. *109*, 771–776.
8. Muro, K., Chung, H.C., Shankaran, V., Geva, R., Catenacci, D., Gupta, S., Eder, J.P., Golan, T., Le, D.T., Burtness, B., et al. (2016). Pembrolizumab for patients with PD-L1-positive advanced gastric cancer (KEYNOTE-012): a multicentre, open-label, phase 1b trial. Lancet Oncol. *17*, 717–726.
9. Brahmer, J.R., Tykodi, S.S., Chow, L.Q., Hwu, W.J., Topalian, S.L., Hwu, P., Drake, C.G., Camacho, L.H., Kauh, J., Odunsi, K., et al. (2012). Safety and activity of anti-PD-L1 antibody in patients with advanced cancer. N. Engl. J. Med. *366*, 2455–2465.
10. Clark, C.E., Hingorani, S.R., Mick, R., Combs, C., Tuveson, D.A., and Vonderheide, R.H. (2007). Dynamics of the immune reaction to pancreatic cancer from inception to invasion. Cancer Res. *67*, 9518–9527.
11. Padoan, A., Plebani, M., and Basso, D. (2019). Inflammation and pancreatic cancer: focus on metabolism, cytokines, and immunity. Int. J. Mol. Sci. *20*, 676.
12. Qu, C., Wang, Q., Meng, Z., and Wang, P. (2018). Cancer-associated fibroblasts in pancreatic cancer: should they be deleted or reeducated? Integr. Cancer Ther. *17*, 1016–1019.
13. Lonardo, E., Frias-Aldeguer, J., Hermann, P.C., and Heeschen, C. (2012). Pancreatic stellate cells form a niche for cancer stem cells and promote their self-renewal and invasiveness. Cell Cycle *11*, 1282–1290.
14. Chiocca, E.A., and Rabkin, S.D. (2014). Oncolytic viruses and their application to cancer immunotherapy. Cancer Immunol. Res. *2*, 295–300.
15. Todo, T., Martuza, R.L., Rabkin, S.D., and Johnson, P.A. (2001). Oncolytic herpes simplex virus vector with enhanced MHC class I presentation and tumor cell killing. Proc. Natl. Acad. Sci. USA *98*, 6396–6401.
16. Jiang, H., Rivera-Molina, Y., Gomez-Manzano, C., Clise-Dwyer, K., Bover, L., Vence, L.M., Yuan, Y., Lang, F.F., Toniatti, C., Hossain, M.B., and Fueyo, J. (2017). Oncolytic adenovirus and tumor-targeting immune modulatory therapy improve autologous cancer vaccination. Cancer Res. *77*, 3894–3907.
17. Hirano, S., Etoh, T., Okunaga, R., Shibata, K., Ohta, M., Nishizono, A., and Kitano, S. (2009). Reovirus inhibits the peritoneal dissemination of pancreatic cancer cells in an immunocompetent animal model. Oncol. Rep. *21*, 1381–1384.

18. Wennier, S.T., Liu, J., Li, S., Rahman, M.M., Mona, M., and McFadden, G. (2012). Myxoma virus sensitizes cancer cells to gemcitabine and is an effective oncolytic virotherapeutic in models of disseminated pancreatic cancer. Mol. Ther. *20*, 759–768.

19. Liu, Z., Ravindranathan, R., Kalinski, P., Guo, Z.S., and Bartlett, D.L. (2017). Rational combination of oncolytic vaccinia virus and PD-L1 blockade works synergistically to enhance therapeutic efficacy. Nat. Commun. *8*, 14754.

20. Eissa, I.R., Bustos-Villalobos, I., Ichinose, T., Matsumura, S., Naoe, Y., Miyajima, N., Morimoto, D., Mukoyama, N., Zhiwen, W., Tanaka, M., et al. (2018). The current status and future prospects of oncolytic viruses in clinical trials against melanoma, glioma, pancreatic, and breast cancers. Cancers (Basel) *10*, 356.

21. Pan, S., Liu, X., Ma, Y., Cao, Y., and He, B. (2018). Herpes simplex virus 1 $\gamma_1$34.5 protein inhibits STING activation that restricts viral replication. J. Virol. *92*, e01015.

22. Oldham, M.L., Hite, R.K., Steffen, A.M., Damko, E., Li, Z., Walz, T., and Chen, J. (2016). A mechanism of viral immune evasion revealed by cryo-EM analysis of the TAP transporter. Nature *529*, 537–540.

23. Johansson, H., Andersson, R., Bauden, M., Hammes, S., Holdenrieder, S., and Ansari, D. (2016). Immune checkpoint therapy for pancreatic cancer. World J. Gastroenterol. *22*, 9457–9476.

24. Qian, B.Z., and Pollard, J.W. (2010). Macrophage diversity enhances tumor progression and metastasis. Cell *141*, 39–51.

25. Sawa-Wejksza, K., and Kandefer-Szerszeń, M. (2018). Tumor-associated macrophages as target for antitumor therapy. Arch. Immunol. Ther. Exp. (Warsz.) *66*, 97–111.

26. Zhao, Y., Zhao, B., Wang, X., Guan, G., Xin, Y., Sun, Y.D., Wang, J.H., Guo, Y., and Zang, Y.J. (2019). Macrophage transcriptome modification induced by hypoxia and lactate. Exp. Ther. Med. *18*, 4811–4819.

27. Mahnke, Y.D., Brodie, T.M., Sallusto, F., Roederer, M., and Lugli, E. (2013). The who's who of T-cell differentiation: human memory T-cell subsets. Eur. J. Immunol. *43*, 2797–2809.

28. Gattinoni, L., Speiser, D.E., Lichterfeld, M., and Bonini, C. (2017). T memory stem cells in health and disease. Nat. Med. *23*, 18–27.

29. Reiser, J., and Banerjee, A. (2016). Effector, memory, and dysfunctional CD8(+) T cell fates in the antitumor immune response. J. Immunol. Res. *2016*, 8941260.

30. Gattinoni, L., Ji, Y., and Restifo, N.P. (2010). Wnt/β-catenin signaling in T-cell immunity and cancer immunotherapy. Clin. Cancer Res. *16*, 4695–4701.

31. Kim, H.J., and Cantor, H. (2014). CD4 T-cell subsets and tumor immunity: the helpful and the not-so-helpful. Cancer Immunol. Res. *2*, 91–98.

32. Kumanogoh, A., Wang, X., Lee, I., Watanabe, C., Kamanaka, M., Shi, W., Yoshida, K., Sato, T., Habu, S., Itoh, M., et al. (2001). Increased T cell autoreactivity in the absence of CD40-CD40 ligand interactions: a role of CD40 in regulatory T cell development. J. Immunol. *166*, 353–360.

33. Kitz, A., and Dominguez-Villar, M. (2017). Molecular mechanisms underlying Th1-like Treg generation and function. Cell. Mol. Life Sci. *74*, 4059–4075.

34. Caccamo, N., La Mendola, C., Orlando, V., Meraviglia, S., Todaro, M., Stassi, G., Sireci, G., Fournié, J.J., and Dieli, F. (2011). Differentiation, phenotype, and function of interleukin-17-producing human Vγ9Vδ2 T cells. Blood *118*, 129–138.

35. Wakimoto, H., Kesari, S., Farrell, C.J., Curry, W.T., Jr., Zaupa, C., Aghi, M., Kuroda, T., Stemmer-Rachamimov, A., Shah, K., Liu, T.C., et al. (2009). Human glioblastoma-derived cancer stem cells: establishment of invasive glioma models and treatment with oncolytic herpes simplex virus vectors. Cancer Res. *69*, 3472–3481.

36. Greig, S.L. (2016). Talimogene Laherparepvec: first global approval. Drugs *76*, 147–154.

37. Kasuya, H., Nishiyama, Y., Nomoto, S., Goshima, F., Takeda, S., Watanabe, I., Nomura, N., Shikano, T., Fujii, T., Kanazumi, N., and Nakao, A. (2007). Suitability of a US3-inactivated HSV mutant (L1BR1) as an oncolytic virus for pancreatic cancer therapy. Cancer Gene Ther. *14*, 533–542.

38. Yamamura, K., Kasuya, H., Sahin, T.T., Tan, G., Hotta, Y., Tsurumaru, N., Fukuda, S., Kanda, M., Kobayashi, D., Tanaka, C., et al. (2014). Combination treatment of human pancreatic cancer xenograft models with the epidermal growth factor receptor tyrosine kinase inhibitor erlotinib and oncolytic herpes simplex virus HF10. Ann. Surg. Oncol. *21*, 691–698.

39. Gayral, M., Lulka, H., Hanoun, N., Biollay, C., Sèlves, J., Vignolle-Vidoni, A., Berthommé, H., Trempat, P., Epstein, A.L., Buscail, L., et al. (2015). Targeted oncolytic herpes simplex virus type 1 eradicates experimental pancreatic tumors. Hum. Gene Ther. *26*, 104–113.

40. Spear, M.A., Sun, F., Eling, D.J., Gilpin, E., Kipps, T.J., Chiocca, E.A., and Bouvet, M. (2000). Cytotoxicity, apoptosis, and viral replication in tumor cells treated with oncolytic ribonucleotide reductase-defective herpes simplex type 1 virus (hrR3) combined with ionizing radiation. Cancer Gene Ther. *7*, 1051–1059.

41. Reinblatt, M., Pin, R.H., Bowers, W.J., Federoff, H.J., and Fong, Y. (2005). Herpes simplex virus amplicon delivery of a hypoxia-inducible soluble vascular endothelial growth factor receptor (sFlk-1) inhibits angiogenesis and tumor growth in pancreatic adenocarcinoma. Ann. Surg. Oncol. *12*, 1025–1036.

42. Lee, J.W., Komar, C.A., Bengsch, F., Graham, K., and Beatty, G.L. (2016). Genetically Engineered Mouse Models of Pancreatic Cancer: The KPC Model (LSL-Kras(G12D/+) ;LSL-Trp53(R172H/+) ;Pdx-1-Cre), Its Variants, and Their Application in Immuno-oncology Drug Discovery. Curr. Protoc. Pharmacol. *73*, 14.39.1–14.39.20.

43. Saha, D., Martuza, R.L., and Rabkin, S.D. (2017). Macrophage polarization contributes to glioblastoma eradication by combination immunovirotherapy and immune checkpoint blockade. Cancer Cell *32*, 253–267.e5.

44. Bommareddy, P.K., Aspromonte, S., Zloza, A., Rabkin, S.D., and Kaufman, H.L. (2018). MEK inhibition enhances oncolytic virus immunotherapy through increased tumor cell killing and T cell activation. Sci. Transl. Med. *10*, eauu0417.

45. Moesta, A.K., Cooke, K., Piasecki, J., Mitchell, P., Rottman, J.B., Fitzgerald, K., Zhan, J., Yang, B., Le, T., Belmontes, B., et al. (2017). Local Delivery of OncoVEXmGM-CSF Generates Systemic Antitumor Immune Responses Enhanced by Cytotoxic T-Lymphocyte-Associated Protein Blockade. Clin. Cancer Res. *23*, 6190–6202.

46. Karamitopoulou, E. (2019). Tumour microenvironment of pancreatic cancer: immune landscape is dictated by molecular and histopathological features. Br. J. Cancer *121*, 5–14.

47. Murakami, T., Hiroshima, Y., Matsuyama, R., Homma, Y., Hoffman, R.M., and Endo, I. (2019). Role of the tumor microenvironment in pancreatic cancer. Ann. Gastroenterol. Surg. *3*, 130–137.

48. Cannarile, M.A., Weisser, M., Jacob, W., Jegg, A.M., Ries, C.H., and Rüttinger, D. (2017). Colony-stimulating factor 1 receptor (CSF1R) inhibitors in cancer therapy. J. Immunother. Cancer *5*, 53.

49. Choi, I.K., Strauss, R., Richter, M., Yun, C.O., and Lieber, A. (2013). Strategies to increase drug penetration in solid tumors. Front. Oncol. *3*, 193.

50. Ganesh, S., Gonzalez-Edick, M., Gibbons, D., Van Roey, M., and Jooss, K. (2008). Intratumoral coadministration of hyaluronidase enzyme and oncolytic adenoviruses enhances virus potency in metastatic tumor models. Clin. Cancer Res. *14*, 3933–3941.

51. McKee, T.D., Grandi, P., Mok, W., Alexandrakis, G., Insin, N., Zimmer, J.P., Bawendi, M.G., Boucher, Y., Breakefield, X.O., and Jain, R.K. (2006). Degradation of fibrillar collagen in a human melanoma xenograft improves the efficacy of an oncolytic herpes simplex virus vector. Cancer Res. *66*, 2509–2513.

52. Jung, B.K., Ko, H.Y., Kang, H., Hong, J., Ahn, H.M., Na, Y., Kim, H., Kim, J.S., and Yun, C.O. (2020). Relaxin-expressing oncolytic adenovirus induces remodeling of physical and immunological aspects of cold tumor to potentiate PD-1 blockade. J. Immunother. Cancer *8*, e000763.

53. Wang, Y., Yang, Y., Wu, S., Pan, S., Zhou, C., Ma, Y., Ru, Y., Dong, S., He, B., Zhang, C., and Cao, Y. (2014). p32 is a novel target for viral protein ICP34.5 of herpes simplex virus type 1 and facilitates viral nuclear egress. J. Biol. Chem. *289*, 35795–35805.

54. Li, S.Y., Du, M.J., Wan, Y.J., Lan, B., Liu, Y.H., Yang, Y., Zhang, C.Z., and Cao, Y. (2013). The N-terminal 20-amino acid region of guanine nucleotide exchange factor Vav1 plays a distinguished role in T cell receptor-mediated calcium signaling. J. Biol. Chem. *288*, 3777–3785.

55. Wan, Y.J., Yang, Y., Leng, Q.L., Lan, B., Jia, H.Y., Liu, Y.H., Zhang, C.Z., and Cao, Y. (2014). Vav1 increases Bcl-2 expression by selective activation of Rac2-Akt in leukemia T cells. Cell. Signal. *26*, 2202–2209.

56. Rich, J.T., Neely, J.G., Paniello, R.C., Voelker, C.C., Nussenbaum, B., and Wang, E.W. (2010). A practical guide to understanding Kaplan-Meier curves. Otolaryngol. Head Neck Surg. *143*, 331–336.

57. Butler, A., Hoffman, P., Smibert, P., Papalexi, E., and Satija, R. (2018). Integrating single-cell transcriptomic data across different conditions, technologies, and species. Nat. Biotechnol. *36*, 411–420.

58. Gu, Z., Eils, R., and Schlesner, M. (2016). Complex heatmaps reveal patterns and correlations in multidimensional genomic data. Bioinformatics *32*, 2847–2849.

59. Yu, G., Wang, L.G., Han, Y., and He, Q.Y. (2012). clusterProfiler: an R package for comparing biological themes among gene clusters. OMICS *16*, 284–287.

60. Rybarczyk, B.J., Walton, K.L.W., and Grillo, W.H. (2014). The development and implementation of an instrument to assess students' data analysis skills in molecular biology. J. Microbiol. Biol. Educ. *15*, 259–267.